Volume 3 | Number 27 | 21 July 2015 | Pages 5379–5646

Journal of Materials Chemistry B

Materials for biology and medicine

www.rsc.org/MaterialsB

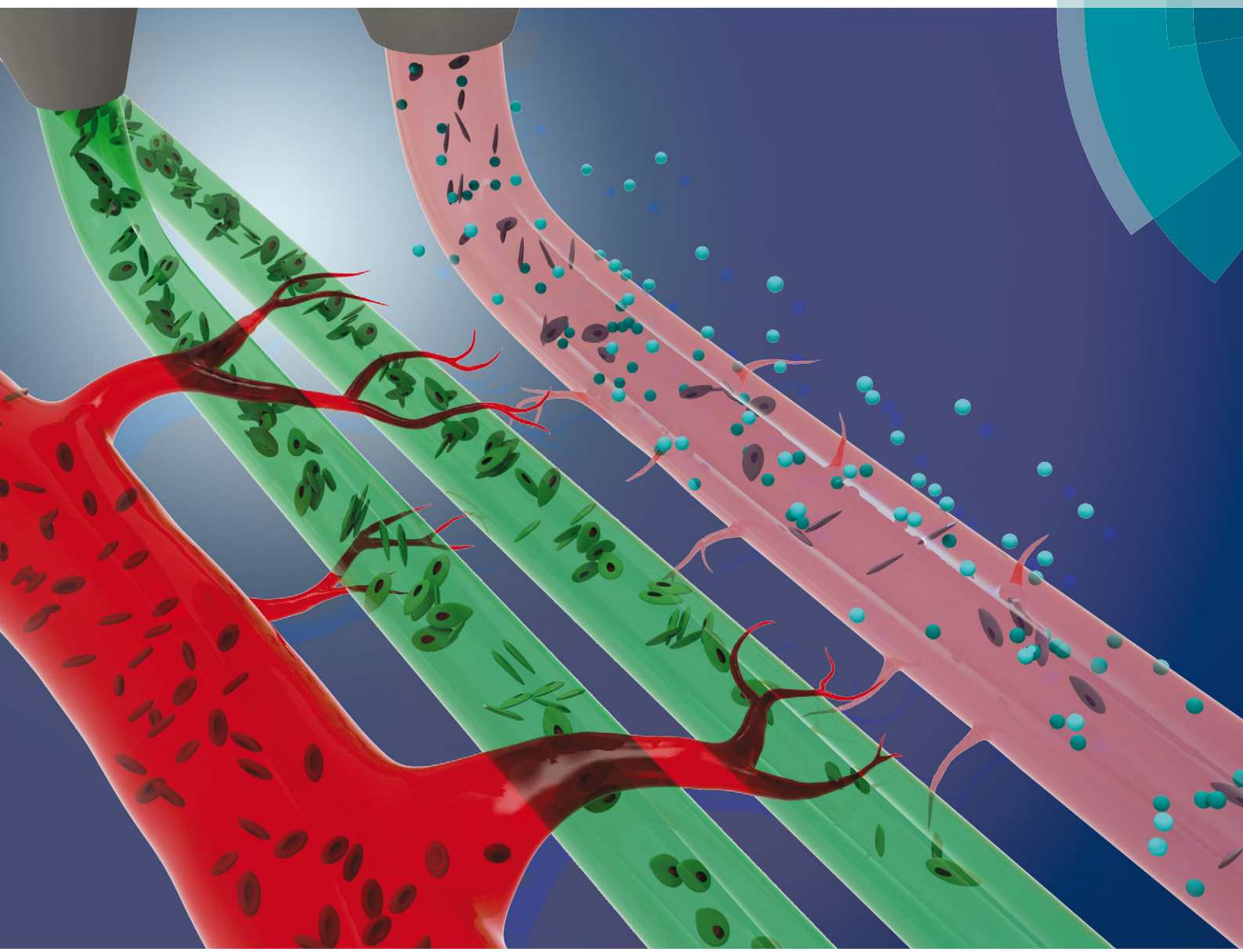

ISSN 2050-750X

ROYAL SOCIETY OF CHEMISTRY

PAPER

Sang Hwa Lee, Dong-Woo Cho *et al.*

3D printing technology to control BMP-2 and VEGF delivery spatially and temporally to promote large-volume bone regeneration

Journal of Materials Chemistry B

PAPER

View Article Online
View Journal | View Issue

Cite this: J. Mater. Chem. B, 2015, 3, 5415

3D printing technology to control BMP-2 and VEGF delivery spatially and temporally to promote large-volume bone regeneration

Ju Young Park,†[a] Jin-Hyung Shim,†[b] Song-Ah Choi,[a] Jinah Jang,[a] Myungshin Kim,[c] Sang Hwa Lee*[d] and Dong-Woo Cho*[e]

Received 7th April 2015,
Accepted 22nd May 2015

DOI: 10.1039/c5tb00637f

www.rsc.org/MaterialsB

When large engineered tissue structures are used to achieve tissue regeneration, formation of vasculature is an essential process. We report a technique that combines 3D printing with spatial and temporal control of dual growth factors to prevascularize bone tissue. Human dental pulp stem cells (DPSCs) that have both osteogenic and vasculogenic potential were printed with bone morphogenetic protein-2 (BMP-2) in the peripheral zone of the 3D printed construct, and with the vascular endothelial growth factor (VEGF) in the central zone, in which a hypoxic area forms. The structure was implanted in the back of a mouse and tissue regeneration was assessed after 28 d. Microvessels were newly formed in the hypoxic area of the printed large volume structure, and angiogenesis from the host tissue was also observed. Bone regeneration was faster in prevascularized structures than in nonvascularized structures. The 3D-printed prevascularized structure could be a promising approach to overcome the size limitation of tissue implants and to enhance bone regeneration.

1. Introduction

Repair of large bone defects is a major challenge in reconstructive surgery. This surgery entails use of grafts, but the process has encountered limitations. Autologous bone is the ideal graft material, because it is the only material with all of osteogenesis, osteoconduction and osteoinduction potentials.[1,2] Use of autologous grafts such as vascular-free flaps improves the clinical outcome of large bone reconstruction, but this method has limitations, including significant donor site morbidity, long operating time, and high cost.[3–6] Allografts, xenografts and synthetic grafts have also been used in bone tissue engineering, but their applicability is limited by lack of osteogenic potential in cells within the graft material.[1,7–10] Several techniques to seed stem cells into the graft materials have been reported, but in these methods cell survival in the deep portion of large scaffolds is compromised due to poor vascularization and consequent hypoxia and insufficient nutrient delivery.[11–13] To achieve rapid angiogenesis into the graft materials, several studies have used co-culture methods (osteogenic and angiogenic cells) and delivery of dual growth factors (osteogenic and angiogenic factors) to enhance vascularization into grafted materials.[14–17] However, bone regeneration studies consistently encounter difficulties when attempting to induce site-specific pharmacological actions of growth factors and consequent anatomically-appropriate arrangement of cells.

Three-dimensional (3D) printing technology is a manufacturing method that uses a layer-by-layer process to build objects. In the context of tissue engineering, 3D printing technology can dispense various functional growth factors, and even live cells with hydrogel, at the desired position until the 3D tissue is built up. Therefore, 3D printing can produce structures that have the spatial features of the native tissue.[18–20]

Mesenchymal dental pulp derived stem cells (DPSCs) from extracted third molars are promising sources of multipotent stromal cells in tissue engineering. Accessibility to the extraction site is easy and those processes present very low morbidity at the donor site. Use of DPSCs has the additional advantage that the production yield of cells from the specimen is high.[21–24] DPSCs can differentiate into both osteoblast and odontoblast lineages,[25] and have higher osteogenic potential than do mesenchymal stem cells derived from the bone marrow.[26] In particular, DPSCs can

[a] Division of Integrative Biosciences and Biotechnology, POSTECH, Pohang, Korea
[b] Department of Mechanical Engineering, Korea Polytechnic University, Siheung, Korea
[c] Department of Laboratory Medicine, Seoul St. Mary's Hospital, The Catholic University of Korea, Seoul, Korea
[d] Department of Oral and Maxillofacial Surgery, Yeouido St. Mary's Hospital, The Catholic University of Korea, 10, 63-ro, Yeongdeungpo-gu, Seoul, 150-713, Korea. E-mail: justina@catholic.ac.kr; Fax: +82-2-769-1689; Tel: +82-2-3779-2148
[e] Department of Mechanical Engineering, Pohang University of Science and Technology (POSTECH), 77 Cheongam-ro, Nam-gu, Pohang, Kyungbuk 790-784, Korea. E-mail: dwcho@postech.ac.kr; Fax: +82-54-279-5419; Tel: +82-54-279-2171
† These authors contributed equally to this work as first authors.

generate vessel-integrated bone tissue structures, which are essential for large volume bone reconstruction.[21]

In the present study, we used 3D printing to fabricate a scaffold laden with DPSCs and spiked with bone morphogenetic protein 2 (BMP-2) and vascular endothelial growth factor (VEGF). The materials used as the scaffold were chosen such that they release BMP-2 slowly and VEGF quickly. BMP-2 was printed in the periphery zone of the 3D printed construct, and VEGF was printed in the central zone, in which a hypoxic area forms. To induce differentiation of bones and vascular tissue, DPSCs, which have a high ability to differentiate into these tissues, were co-printed with each growth factor in each, and then the formation of each tissue was evaluated. We hypothesized that the VEGF printed in the central zone may facilitate early vasculogenesis of DPSC and thereby result in sufficient blood vessel formation, which might promote bone formation even in the core of a large structure.

2. Materials and methods

2.1. Regulation of the profiling of the growth factors for bone and vascular regeneration

To regulate the release profile of each growth factor, 2% (w/v) collagen type I hydrogel (Koken Co. Ltd, Tokyo, Japan) was used to obtain sustained release of BMP-2 (5 μg mL^{-1}) to induce bone regeneration, and mixed hydrogel with 10% (w/v) alginate and 10% (w/v) gelatin was used to obtain burst release of VEGF (2 μg mL^{-1}) to induce vascularization. The 3D structure was fabricated by 3D printing technology using the multi-head tissue/organ building system which was developed in our lab.[27] Polycaprolactone (PCL; MW 65 000, Sigma-Aldrich, St. Louis, MO, USA) was melted at 130 °C and dispensed by controlled pneumatic pressure with a line width of 200 μm and a line height of 100 μm and a total of twelve PCL lines were printed in parallel with a gap diameter of 400 μm between PCL lines, to make the frameworks. Then growth factors encapsulated in each hydrogel were filled into every second gap between PCL lines (Fig. 1). The dispensed collagen hydrogel was gelled at 37 °C in 5% CO_2 in an incubator for 30 min. The alginate–gelatin mixture was crosslinked by incubation with 2% (w/v) $CaCl_2$ solution at 37 °C in 5% CO_2 in an incubator for 15 min. That is, only the alginate part was crosslinked; to allow burst release of VEGF, the gelatin part was left without the crosslinking process.

2.1.1. Evaluation of the release profile. To evaluate the release profile, each structure was incubated in 10 mL of phosphate buffer saline (PBS) buffer, and the supernatant was collected every day for 40 d. The supernatant was analyzed using enzyme-linked immunosorbent assay (ELISA) to assess the release profiles of BMP-2 and VEGF from each structure.

2.2. Printing of the structure with DPSCs and growth factors for *in vitro* study

DPSCs were isolated as previously described.[28] The cell isolation protocol was approved (approval no. SC11TISE0046) by the Institutional Review Board of the St. Mary's Hospital the Catholic University of Korea. DPSCs were cultured in Alpha-modified Eagle's medium (α-MEM; Gibco BRL, Grand Island, NY, USA) supplemented with 10% (v/v) fetal bovine serum (FBS; Gibco BRL), 100 U mL^{-1} penicillin (Gibco BRL), and 0.1 mg mL^{-1} streptomycin (Gibco BRL) (Complete α-MEM media). The culture media were changed every 2 d; 0.05% trypsin (Gibco BRL) was used to detach the cells from the culture dish.

DPSCs were encapsulated within 2% collagen type I hydrogel with BMP-2, and within 10% gelatin/10% alginate mixed hydrogel with VEGF (2×10^6 cells per mL). Then the mixture (cells and hydrogel solution) was moved to a plastic syringe (10 cc) equipped with tapered plastic nozzle (200 μm). Pneumatic pressure (30–50 kPa) was applied to dispense the cell–hydrogel

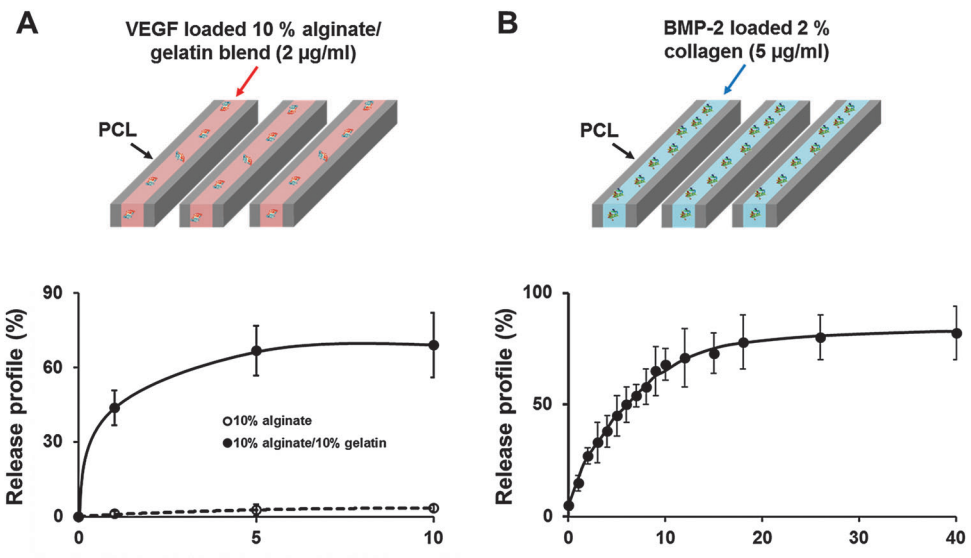

Fig. 1 Release profile from the 3D structure printed with (A) VEGF using 10% alginate/10% gelatin blended gel (red arrow) and PCL framework (black arrow), (B) BMP-2 using 2% collagen gel (blue arrow) and PCL framework (black arrow).

solution mixture. At that time, the printing nozzle was moved at 50–100 mm min^{-1}. The dispensed cell–Col-1 and cell–alginate–gelatin mixtures were crosslinked as mentioned above. The 3D structure in which the cells and growth factors were printed was cultured in complete α-MEM for 14 d to evaluate the viability of DPSCs after printing and the capacity of the 3D structure to differentiate into each tissue.

2.2.1. Evaluation of the cell survival rate. First, the survival rate of printed DPSCs was measured using a live/dead cell assay kit (Lonza, Walkersville, MD, USA) at 24 h after printing. Calcein AM and ethidium homodimer (EthD-1) were mixed in α-MEM medium supplemented with 2% (v/v) FBS and the mixture was added to cell printed structures, then incubated at 37 °C in 5% CO_2 in an incubator for 15 min. Live and dead cells were observed under a fluorescence microscope (IX81, Olympus, Tokyo, Japan), calcein AM (green) indicated live cells and EthD-1 (red) indicated dead cells.

2.2.2. Analysis of vasculogenic and osteogenic differentiation. To quantify how the release profiles of the growth factors affected DPSC differentiation into bone or vessel, the marker gene expression of bone and vessel was verified using real-time PCR (qRT-PCR). Trizol Reagent (Invitrogen, Carlsbad, CA) was used to isolate total RNA from the structures, and SuperScript II Reverse Transcriptase (Invitrogen, Carlsbad, CA) was used to reverse-transcribe the RNA to cDNA. Then, expression of bone and vascular marker genes was evaluated using amplification primers (Table 1). The primer for human glyceraldehyde 3-phosphate dehydrogenase (GAPDH) was used to standardize the expression of the other marker genes. qRT-PCR analysis using SYBR Green (Takara Bio, Kyoto, Japan) was conducted using a Light Cycler 2.0 (Roche, Mannheim, Germany).

2.3. *In vivo* study

The structures were fabricated with dimensions of 3.8 × 3.8 × 3.8 mm and 5.6 × 5.6 × 5.6 mm (width × length × height) to define the large volume structure (Fig. 4). For fabrication of a smaller size structure (3.8 × 3.8 × 3.8 mm), PCL lines with a line width of 200 μm and line height of 100 μm were printed with a pore size of 400 μm; 10 layers of PCL frameworks were printed with this layer-by-layer process (55 mm^3). The larger size structure (5.6 × 5.6 × 5.6 mm) was also fabricated with this layer-by-layer process but consisted of 15 layers of PCL frameworks (176 mm^3). To map the hypoxic areas in the structures, DPSCs were seeded onto each structure at a cell density of 2×10^3 cells per mm^3, and they were incubated in a static culture for 3 d; then a hypoxia-sensitive staining solution (Pimonidazole) was applied to the cell culture medium and the structure was incubated for another 36 h. Then the structure was fixed in 10% formalin solution and embedded in a freezing compound (O.C.T. compound, Sakura Finetek Co., Ltd, Tokyo, Japan). The frozen tissue was sliced into 10 μm-thick sections using a cryomicrotome (Leica, Wetzler, Germany), and then Pimonidazole staining was carried out using the Hypoxyprobe-1 Plus Kit (Hypoxyprobe, Inc., Burlington, VT). The tissue slides were treated with 0.01% Triton X-100 for 5 min at room temperature (RT), then blocked with 1% bovine serum albumin for 1 h at RT. An FITC-mouse IgG1 monoclonal antibody was treated with the primary reagent for 16 h at 4 °C. Then the slides were treated with an anti-FITC antibody for 1 h at RT. The slides were mounted and observed under a confocal microscope (FV1000, Olympus, Tokyo, Japan).

To verify that vascular printing affected vascularization in the hypoxic area *in vivo*, three experimental groups were designed (Fig. 5): (1) the structure printed with 2% collagen encapsulating DPSCs, (2) the structure printed with 2% collagen encapsulating DPSCs and BMP-2, and (3) the structure printed with 10% alginate/10% gelatin hydrogel encapsulating DPSCs and VEGF in the hypoxic area of the structure and with 2% collagen encapsulating DPSCs and BMP-2 in the remaining area except the hypoxic area of the structure. The fabricated structures were cultured in complete α-MEM media for 3 d *in vitro*.

Animal tests were performed with the approval (approval no. 2012-01-0017) of the Institutional Animal Care and Use Committee of the Pohang University of Science and Technology (POSTECH), Korea. Ten each of constructs group 1, 2 and 3 were fabricated, and each was implanted subdermally in the back of one of the thirty immunodeficient mice (BALB/c-nu/nu, 25 g, 7 weeks old, female) chosen randomly. After 4 weeks, the structures were harvested and fixed in a 10% formalin solution for 4 h. After washing with PBS, the structures were embedded in O.C.T. Compound, and frozen sections of 10 μm thickness were thaw-mounted on the slides using a cryomicrotome (Leica, Wetzler, Germany). The frozen sections were labeled with BSI (Lectin from *Bandeiraea simplicifolia*; Sigma-Aldrich) to identify

Table 1 PCR primer sequences

Gene		Sequence	Cycles	Melting temperature (°C)
ALP	Sense	ATGTCATCATGTTCCTGGGAGAT	45	95
	Anti-sense	TGGAGCTGACCCTTGAGGAT		
Runx2	Sense	AACCCACGAATGCACTATCCA	45	95
	Anti-sense	CGGACATACCGAGGGACATG		
VE-cadherin	Sense	CCTGATGCGGCTAGGCATA	45	95
	Anti-sense	GGAAGAACTGGCCCTTGTCA		
PECAM	Sense	AAATGATCCTGCGGTATTCAAAG	45	95
	Anti-sense	GCGTGGGAATGGCAATTATC		
VEGFR-2	Sense	CTCACATGGTACAAGCTTGGC	45	95
	Anti-sense	TGCCACACGCTCTAGGACTGT		
GAPDH	Sense	CCAGGTGGTCTCCTCTGACTTC	45	95
	Anti-sense	GTGGTCGTTGAGGGCAATG		

blood endothelial cell differentiation from the encapsulated DPSCs in hydrogel with VEGF. Vascular endothelial (VE)-cadherin, an endothelial specific adhesion molecule, antibody (Abcam, Cambridge, MA, USA) was also used to verify healthy blood vessel formation. Nuclei were counterstained with 4′,6-diamidino-2-phenylindole (DAPI). To identify the cell originality in the host tissue after the structure implantation, tissue sections were incubated with a human-specific Lamin A/C (NCL-Lam-A/C, mouse monoclonal IgG2b, 1:200) antibody to detect human cells. The mounted slides were observed using a confocal microscope (FV1000, Olympus, Tokyo, Japan). Alizarin Red S staining was conducted to assess calcium deposition in the structure to verify the cell differentiation into calcium-secreted mature bone cells. Tissue sections were also stained with Masson's trichrome (MT) to assess collagen deposition. The stained slides were viewed with a light microscope (Axiovert 200 M, Carl Zeiss, Oberkochen, Germany).

2.4. Statistical analysis

All experimental data were expressed as means ± standard deviation from several separate experiments. Statistical analysis was performed *via* one-way analysis of variance (ANOVA) with a post-hoc Tukey test using MINITAB (version 14.2; Minitab, Inc., State College, PA). Differences between experimental groups were considered statistically significant at $p < 0.05$.

3. Results

3.1. Regulation of growth factor release rate for bone and vascular regeneration

According to the ELISA assay; 44% of the total encapsulated VEGF was released just within 1 d, 67% was released within 5 d and 69% was released within 10 d (Fig. 1A). In contrast, BMP-2 was printed using 2% collagen gel to induce a sustained release. In the release profile, 60% of the encapsulated BMP-2 was released within 7 d, and 80.5% was consistently released by 40 d (Fig. 1B).

3.2. Evaluation of the cell survival rate

To test the safety of the cell printing process with each hydrogel, cell viability in each cell-printed structure was evaluated. Cell viability was calculated by counting the live (green) and dead (red) cells. One day after printing, the survival rates of the printed cells with collagen hydrogel and alginate–gelatin mixture were about 92 and 99% respectively (Fig. 2).

3.3. *In vitro* assessment of the growth factor release rate in cell differentiation

VE-Cadherin, PECAM, and VEGFR-2 expression levels in DPSCs printed using 10% alginate/10% gelatin mixed gel with VEGF (2 μg mL^{-1}) were 27, 42, and 34 times higher, respectively, than those without VEGF at 7 d after printing (Fig. 3A). ALP and Runx2 expression levels in DPSCs printed using 2% collagen gel with

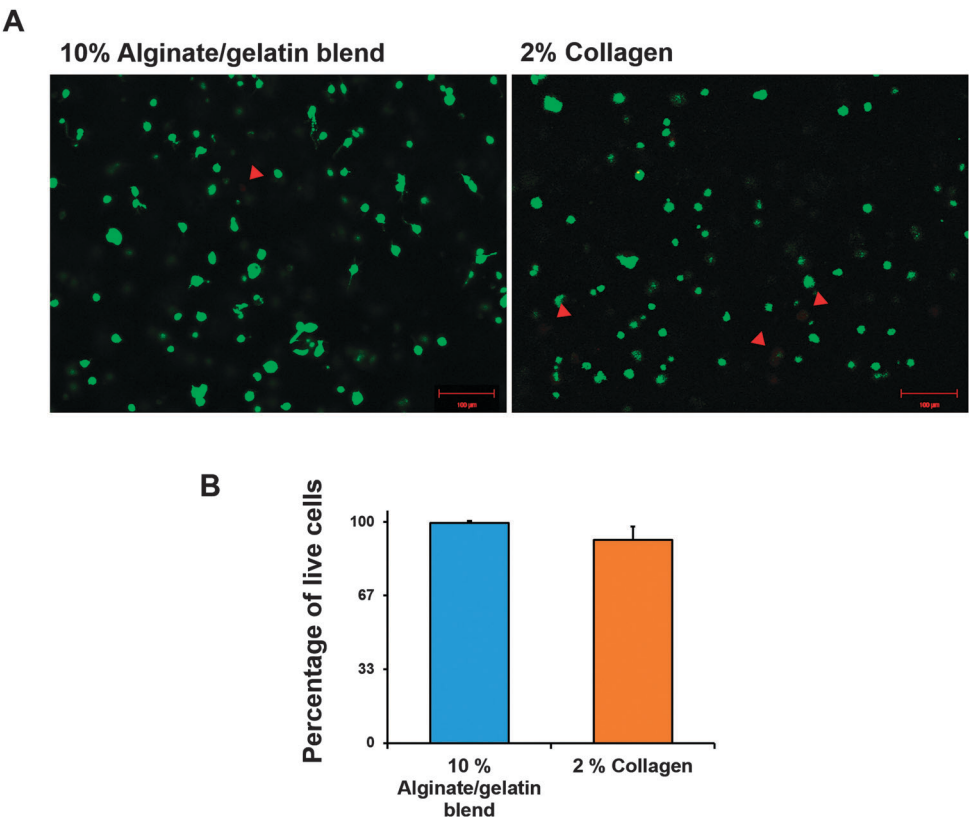

Fig. 2 Survival rate of DPSCs within the 3D printed structure. (A) Confocal imaging of DPSCs stained with fluorescence dyes for a viability assay. Live cells were stained with calcein AM (green) and dead cells were stained with ethidium homodimer (red, red arrow). (B) Percentages of live cells. Scale bar: 100 μm.

BMP-2 (5 μg mL^{-1}) were 2 and 4 times higher at 7 d and 7 and 14 times higher at 14 d after printing, respectively, than those without BMP-2 (Fig. 3B).

Histological characteristics of vessel and bone were affected by the treatments. In the structure in which DPSCs were printed with VEGF using 10% alginate/10% gelatin blended gel, the BSI-Lectin staining revealed subsequent assembly of encapsulated cells into a vascular network. A filopodia-like structure, which is the key morphological characteristic of endothelial tip cells, formed at the edge of the DPSCs just within 1 d, and interconnections between the cells formed in 3 d. Finally, tube-like structures, the marker of the functional vessel, were formed in 5 d (Fig. 4A). In contrast, no vascular network formed from DPSCs in the structure printed using the gel without VEGF (data not shown). DPSCs printed with BMP-2 using 2% collagen gel were strongly stained by Alizarin Red S (Fig. 4B), which is specific for Ca^{2+} deposition; DPSCs printed using 2% collagen without BMP-2 were not positively stained by Alizarin Red S (Fig. 4B). Overall, 2% collagen and 10% alginate/10% gelatin blended gel were suitable for the sustained and burst release of encapsulated growth factor, respectively, and those structures printed with VEGF and BMP-2 were effective in inducing vasculogenic and osteogenic differentiation, respectively, from DPSCs encapsulated in each gel.

3.4. *In vivo* study

3.4.1. Assessment of the hypoxic areas in the printed structure. We postulated that a structure greater than a critical size may need to be prevascularized before it can be used for large volume tissue regeneration. We fabricated structures of two sizes, 3.8 × 3.8 × 3.8 mm and 5.6 × 5.6 × 5.6 mm, to determine the critical size of structure that can cause a hypoxic volume within it (Fig. 5A). No-positively-stained cells were observed in the small structure (3.8 × 3.8 × 3.8 mm) (Fig. 5B(a)); on the other hand, positively-stained (*i.e.*, hypoxic) cells (green fluorescence) were observed in center of the large (5.6 × 5.6 × 5.6 mm) structure (Fig. 5B(c and i)). Therefore, the structure size of 5.6 × 5.6 × 5.6 mm was selected for use in tests to confirm the regeneration of a large volume of prevascularized bone graft.

3.4.2. *In vivo* evaluation of 3D printed prevascularized bone grafts. To verify the effect of spatial and temporal control of growth factors using 3D printing technology on prevascularized large bone regeneration, 3D printed structures were designed and fabricated in three groups (Fig. 6). DPSCs and VEGF encapsulated in 10% alginate/10% gelatin blended gel were printed in the hypoxic area confirmed by the Pimonidazole staining, and DPSCs and BMP-2 encapsulated in 2% collagen gel were printed in the remaining part of the structure of dimensions 5.6 × 5.6 × 5.6 mm (group 3). Control groups were printed only with DPSCs or DPSCs and BMP-2 in the whole area of the structures (groups 1 and 2). The structures were implanted in the backs of the mice, and then harvested 4 weeks later.

Blood vessel formation was observed by BSI-Lectin staining using the structure harvested at 28 d after implantation. Vasculature formation in the center was observed only in the 3D-printed prevascularized structure (group 3) (Fig. 7A). On the other hand, vasculature formation was observed at the boundary area in all groups of the structures (Fig. 7B). The number of vessels formed in the periphery zone of the structures was significantly higher in group 3 than in the other groups (Fig. 7C). These results demonstrate that printed VEGF induced vasculogenesis from the DPSCs in the hypoxic volume, and induced angiogenesis from the host tissue within the periphery zone of the structure.

Bone regeneration was confirmed using MT staining, which dyes collagen tissue blue, to evaluate the effect of prevascularized structure on large-volume bone regeneration. Blue-positive staining, which indicates that the encapsulated cells secreted

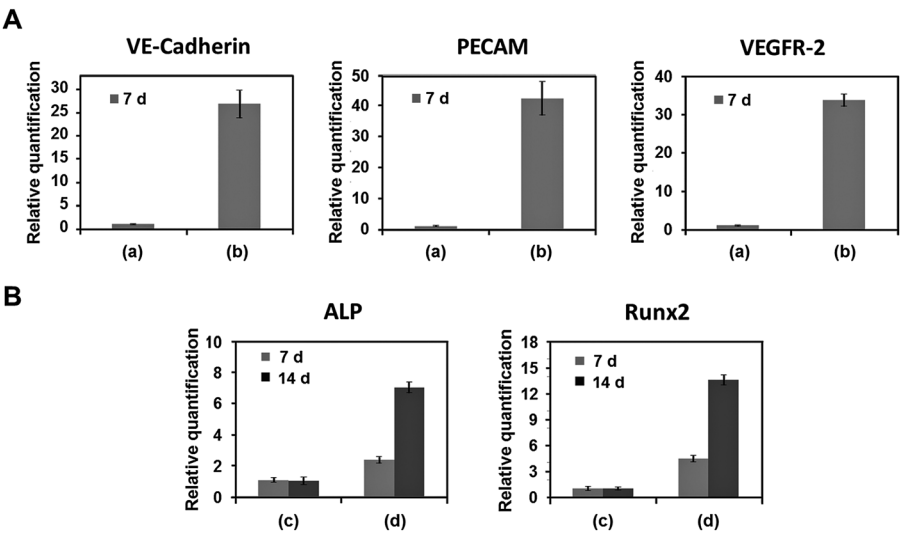

Fig. 3 Assessment of the effect of the release profile on vasculogenic and osteogenic differentiation *in vitro*. Real-time PCR using (A) (a) DPSC printed structure using 10% alginate/10% gelatin blend and (b) DPSCs/VEGF printed structure using 10% alginate/10% gelatin blend. (B) (c) DPSC printed scaffold using 2% collagen and (d) DPSCs/BMP-2 printed structure using 2% collagen.

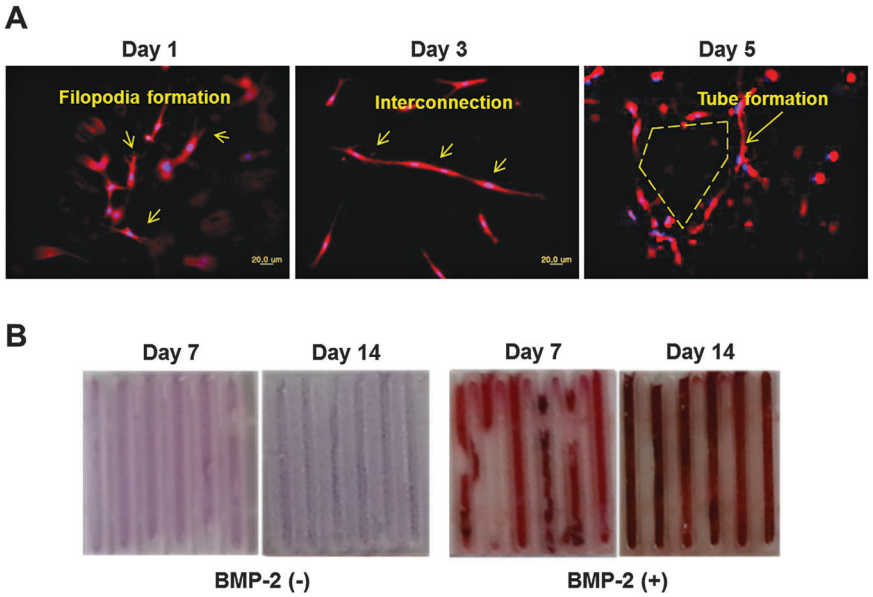

Fig. 4 Histological evaluation of cellular differentiation. (A) BSI-Lectin staining of the structure printed with DPSCs using 10% alginate/10% gelatin blended gel with VEGF. (B) Alizarin Red S staining of the structure printed with DPSCs using 2% collagen with or without BMP-2.

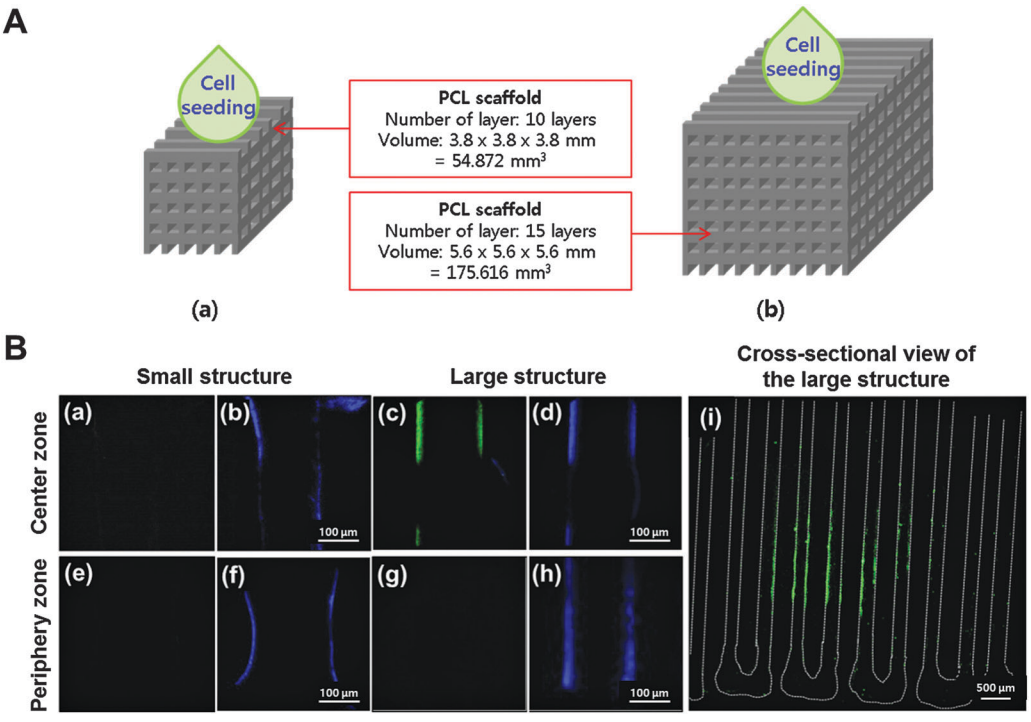

Fig. 5 Pimonidazole staining for the confirmation of a hypoxic area formation in the printed structure. (A) Diagram of the printed structures of (a) the small structure (3.8 × 3.8 × 3.8 mm), and (b) the large structure (5.6 × 5.6 × 5.6 mm) (B). Observation of positive staining with Pimonidazole (green) and DAPI (blue) at the center (a, b) and periphery (e, f) zone of the small structure, and the center (c, d) and periphery (g, h) zone of the large structure under the static culture condition, (i) cross-sectional view of Pimonidazole positive stained area in the large structure.

collagenous proteins, was seldom observed in group 1 and 2, but group 3 showed strong staining (Fig. 8). However, the degree of blue-positive staining in the structure of group 3 was different between the outer and center zones. These differences demonstrate the importance of oxygen and nutrient delivery for induction of tissue regeneration, and suggest that 3D printing technology is useful in inducing formation of blood vessels for large-volume bone regeneration.

We also quantified expression of vascular and bone marker genes in DPSCs transplanted with 3D printed structures *in vivo*

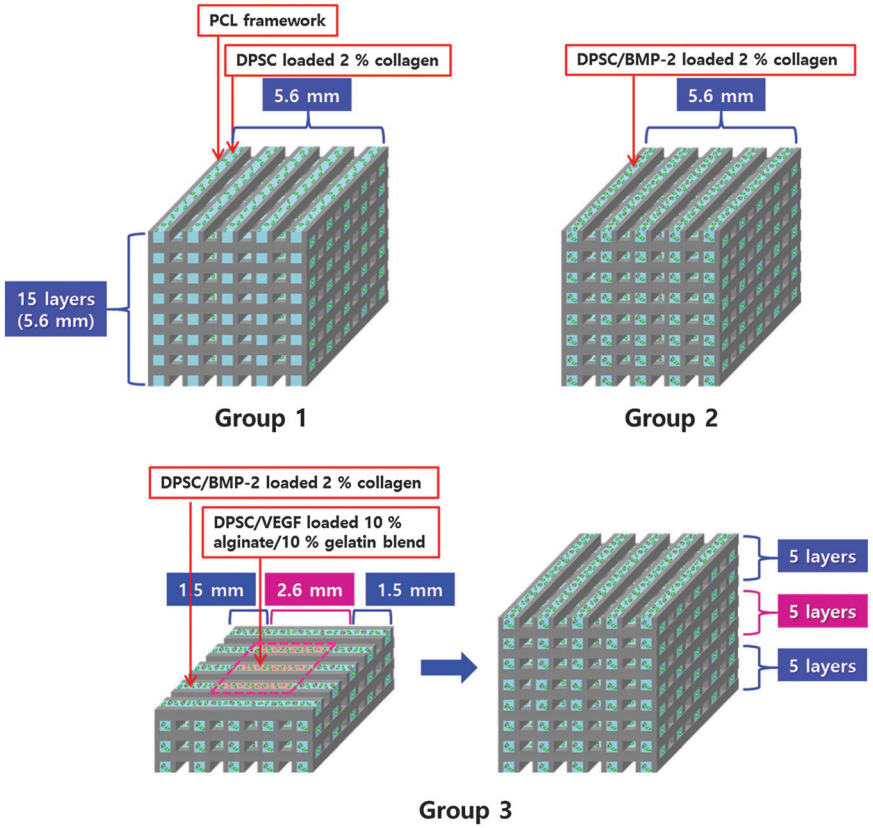

Fig. 6 Structure designs. Group 1: DPSCs printed structure using 2% collagen. Group 2: DPSC/BMP-2 printed structure using 2% collagen. Group 3: DPSC/dual growth factors printed structure using 2% collagen and 10% alginate/10% gelatin blend.

(Fig. 9). Vascular marker genes (VE-Cadherin, PECAM, VEGFR-2) were highly expressed only in the structure of group 3. VE-Cadherin, PECAM, and VEGFR-2 expression levels in group 3 were 2.7, 8.9, and 2.7 times higher, respectively, than those in group 2, but the expression levels did not differ between groups 1 and 2. Bone marker genes (ALP, Runx2) were highly expressed in the structures (groups 2 and 3) that had DPSCs printed with BMP-2 using 2% collagen gel. ALP and Runx2 expression levels in group 2 were 2.7 and 2.0 times higher, respectively, than those in group 1, and those expression levels in group 3 were 1.34 and 1.25 times higher, respectively, than those in group 2 (Fig. 9B). These results suggest that temporally and spatially controllable 3D printing technology is effective for inducing large-volume bone regeneration.

Finally, to determine the effect of the implanted cells on vascular and bone tissue regeneration, the existence of implanted human-derived DPSCs in the implanted structures was confirmed. The structures were labelled using a human specific Lamin A/C antibody for recognizing human cells; positively-stained cells were highly expressed in the inner and periphery zones of the structure of group 3; a much smaller number of positively-stained cells were observed in the center and periphery zones of the structures of group 2 and in the periphery zone of the structure of group 1. Positively-stained cells were not observed at the center zone in the structure of group 1 (Fig. 10). These results suggest that printing structure, especially the prevascularized part, might have a strong influence on the survival of transplanted DPSCs.

4. Discussion

Artificial vessel formation in a graft is essential to regenerate both a large volume of tissue and to promote vascular tissue integration with the host.[29] Therefore, many researchers have tried to fabricate prevascularized artificial grafts. One approach is to use human mesenchymal stem cells (hMSCs) and endothelial cells derived from the umbilical cord and to combine them with a fibronectin-containing collagen gel to generate vascularized bone grafts; the hMSCs present both osteogenic potential and perivascular feature, and the endothelial cells form tube-like structures and subsequently networks throughout the bone scaffold.[30] Another strategy uses dual growth factors (BMP-2 and VEGF) to regenerate vascularized bone; BMP-2 is an effective osteogenic growth factor that is widely used in bone tissue engineering, and VEGF is a potent vasculogenic factor that participates in repair of damaged bone.[31] Dual delivery of BMP-2 and VEGF had a synergistic effect on bone formation in a critical-size rat cranial defect.[14] Sequential delivery of VEGF and BMP-2 can enhance bone regeneration;[32,33] in these studies, the release rate of VEGF was designed to be rapid and that of BMP-2 was designed to be sustained. However, the usefulness of

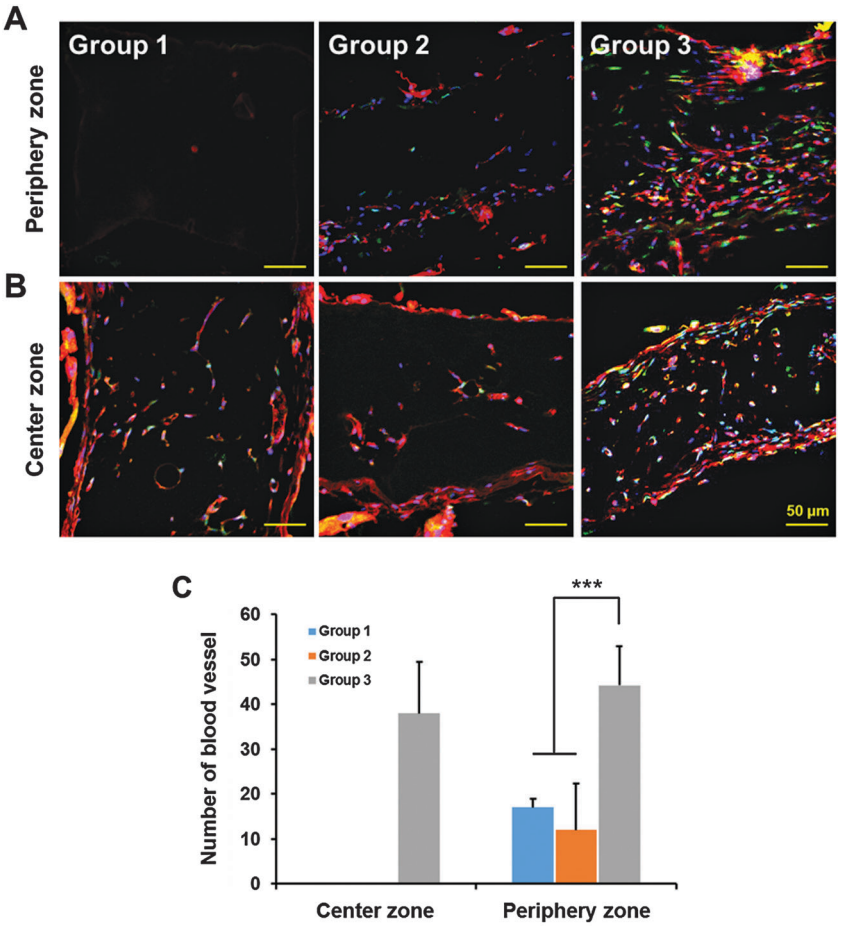

Fig. 7 Vessel formation in the implanted structures. Observation of positive staining with BSI-Lectin (red), VE-cadherin (green), and DAPI (blue) at the (A) center and (B) periphery zone of the printed structure of groups 1, 2, and 3. (C) Average number of blood vessels per 0.1 mm^2 at three different sites in the implanted structures. Bars: ±1 s.d., $n = 3$; *** $p < 0.001$.

these methods can be limited when researchers want to obtain large-volume tissue regeneration because large structures cannot be built of hydrogel alone and therefore cannot have sufficient mechanical strength to support bone tissue regeneration.

In the present study, large-volume structures for grafting into bone defects were fabricated by 3D printing, and stem cells and dual growth factors were deposited within gel matrices that were engineered to release the factors in patterns that were specified temporally and spatially to induce bone regeneration effectively (Fig. 6). To assess the temporal control of the releasing speed of dual growth factors on tissue regeneration, use the 3D printing system to print two hydrogels: collagen loaded with recombinant human BMP-2 (rhBMP-2) gelated at 37 °C and an alginate–gelatin loaded with VEGF prepared by simple blending, with the crosslinking process using $CaCl_2$ solution for gelation of only alginate part. Therefore, the non-crosslinked components were easily diluted by the culture media, thereby leading to rapid release of VEGF from the gelatin (Fig. 1A), whereas the release of BMP-2 from the crosslinked 2% collagen gel was slow (Fig. 1B). The printing of VEGF in only the center of the structure ensured reduction in the total amount of VEGF used; this reduction in amount is necessary because excessive VEGF is strongly correlated to tumour formation.[34–36]

We also hypothesised that printing VEGF only in the center would result in the formation of a concentration gradient of the released VEGF from the center towards the periphery of the structure, and that this gradient would induce angiogenesis from the host tissue. By exploiting the temporal and spatial control, fast neovascularization can be induced from the printed VEGF and stem cells in the center volume of the large 3D scaffold in which hypoxic conditions may occur (Fig. 4); this vascularization might lead to high viability of printed cells in the center of the structure, and thereby help to promote angiogenesis from the host tissue into the implanted artificial bone graft without formation of an aberrant vasculature (Fig. 7, group 3).

In addition, observations confirmed that spontaneous angiogenesis occurred in the periphery portions of the scaffold, but not in the center part as the scaffold size increased (Fig. 7A, group 1). Staining of newly-developed vascular tissue in the center part showed a tube-like shape, presumed to be internal movement of red blood cells, thus possibly confirming that blood was being pumped into the blood vessels. Finally, we confirmed

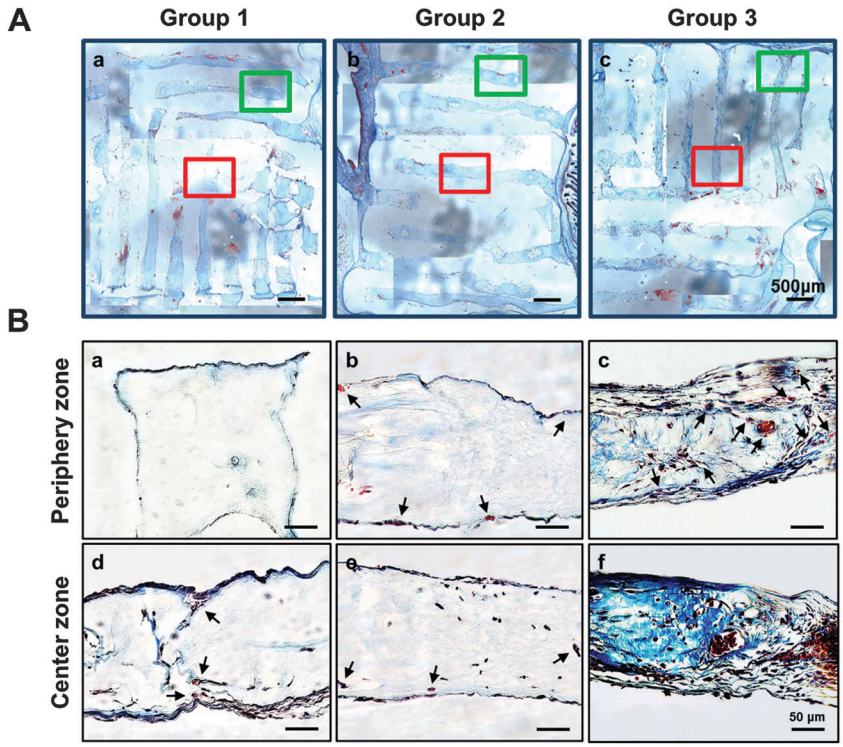

Fig. 8 Masson's trichrome staining. (A) A cross-sectional view of the structures of group 1 (a), 2 (b), and 3 (c), (red box: central, green box: periphery zone where the pictures were taken) (B). Observation of center and periphery zone (red and green boxes in (A)) in the structure of group 1, (a, d) group 2 (b, c), and group 3 (c, f).

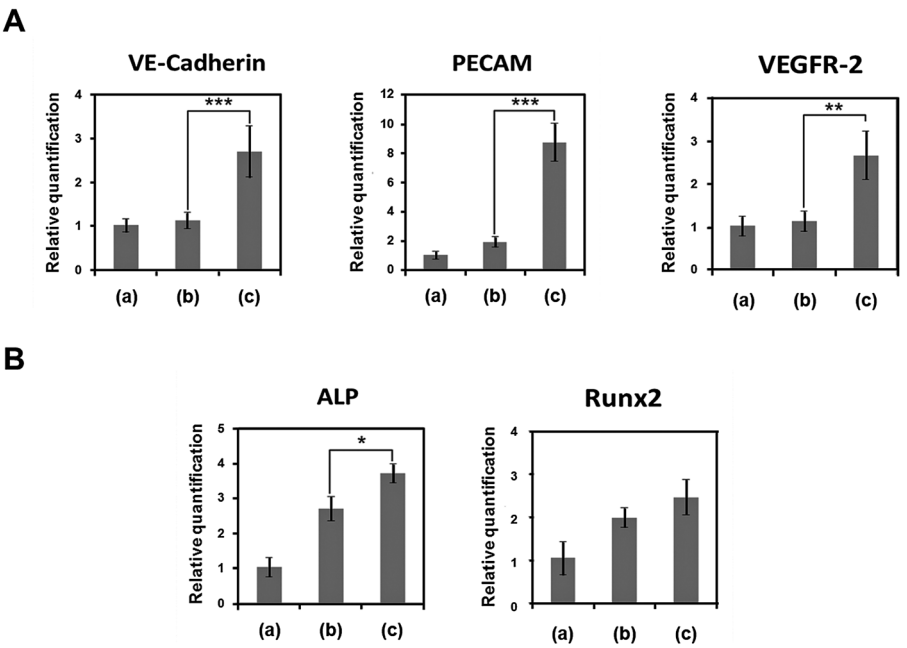

Fig. 9 Induction of osteogenic and vasculogenic differentiation in the 3D printed structures *in vivo*. Real-time PCR using (A) vasculogenic gene primers and (B) osteogenic gene primers using the 3D printed structures of group (a) 1, (b) 2, and (c) 3 at 4 weeks after implantation in the backs of mice. Bars: ±1 s.d., $n = 3$; *: $p < 0.05$; **: $p < 0.005$; ***: $p < 0.001$.

enhanced bone tissue regeneration in the prevascularized structures by assessing deposition of the collagen and marker gene expression compared to the other groups (Fig. 8). The promoting effect on bone tissue regeneration would be affected by the vascularization as well as by the BMP-2. Therefore, this study demonstrates the importance of oxygen and nutrient

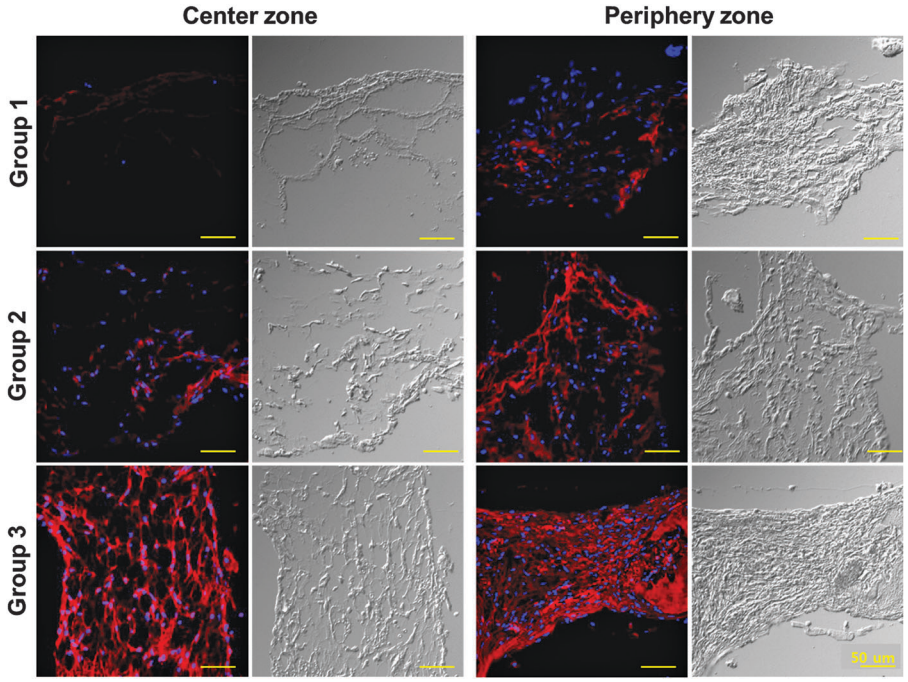

Fig. 10 The existence of DPSCs in the printed structure at 28 days after implantation. The observation of positive staining with DAPI (blue) and human specific Lamin A/C antibody (red) at the center and periphery zone in the structures of experimental group 1, 2, and 3, respectively. The parallel images on the right side of the stained pictures show the phase contrast images.

delivery for the induction of tissue regeneration, and suggests that 3D printing technology is a useful technology to construct structures that can be used to induce formation of blood vessels for large-volume bone regeneration.

5. Conclusion

We demonstrated that multi-head 3D printing technology could control the position and release speed of two growth factors (VEGF, and BMP-2) with dental pulp stem cells (DPSCs) for vascularized bone tissue engineering. In particular, the printed VEGF in the hypoxic center of a large scaffold induced fast neovascularization from DPSCs, by which process the hypoxic condition was alleviated. We believe that the 3D printing technology enabling spatial and temporal control of various growth factors and cells could be extensively applied to heterogeneous tissue engineering. Future work will focus on pre-clinical evaluation of the 3D-printed structure for regeneration of heterogeneous tissues in large animals.

Acknowledgements

This work was supported by the National Research Foundation of Korea (NRF) grant funded by the Korea government (MSIP) (No. 2010-0018294), the R&D program of MSIP/COMPA (No. 2014K000163), Institute of Clinical Medicine Research Yeouido St. Mary's Hospital, and the Academic Promotion System of Korea Polytechnic University.

References

1 R. Dimitriou, E. Jones, D. McGonagle and P. V. Giannoudis, *BMC Med.*, 2011, **9**, 66.
2 P. V. Giannoudis, H. Dinopoulos and E. Tsiridis, *Injury*, 2005, **36**, 20–27.
3 G. G. Kim, A. X. Hang, C. A. Mitchell and A. M. Zanation, *Adv. Oto-Rhino-Laryngol.*, 2013, **74**, 71–80.
4 S. G. Kwon, Y. O. Kim and D. K. Rah, *Arch. Plast. Surg.*, 2012, **39**, 345–351.
5 W. S. Khan, F. Rayan, B. S. Dhinsa and D. Marsh, *Stem Cells Int.*, 2012, **2012**, 236231.
6 C. E. Schwartz, J. F. Martha, P. Kowalski, D. A. Wang, R. Bode, L. Li and D. H. Kim, *Health Qual. Life Outcomes*, 2009, **7**, 49.
7 Z. Bagher, F. Rajaei and M. Shokrgozar, *Iran. Biomed. J.*, 2012, **16**, 18–24.
8 D. M. Ehrler and A. R. Vaccaro, *Clin. Orthop. Relat. Res.*, 2000, 38–45.
9 C. G. Finkemeier, *J. Bone Jt. Surg., Am. Vol.*, 2002, **84A**, 454–464.
10 C. A. Vacanti, L. J. Bonassar, M. P. Vacanti and J. Shufflebarger, *N. Engl. J. Med.*, 2001, **344**, 1511–1514.
11 A. G. Ardakani, U. Cheema, R. A. Brown and R. J. Shipley, *J. R. Soc., Interface*, 2014, **11**, 20140501.
12 S. Seitz, K. Ern, G. Lamper, D. Docheva, I. Drosse, S. Milz, W. Mutschler and M. Schieker, *Tissue Eng.*, 2007, **13**, 1059–1067.
13 E. Volkmer, I. Drosse, S. Otto, A. Stangelmayer, M. Stengele, B. C. Kallukalam, W. Mutschler and M. Schieker, *Tissue Eng., Part A*, 2008, **14**, 1331–1340.
14 Z. S. Patel, S. Young, Y. Tabata, J. A. Jansen, M. E. Wong and A. G. Mikos, *Bone*, 2008, **43**, 931–940.

15 J. Rouwkema, J. de Boer and C. A. Van Blitterswijk, *Tissue Eng.*, 2006, **12**, 2685–2693.
16 M. Samee, S. Kasugai, H. Kondo, K. Ohya, H. Shimokawa and S. Kuroda, *J. Pharmacol. Sci.*, 2008, **108**, 18–31.
17 W. Thein-Han and H. H. Xu, *Tissue Eng., Part A*, 2013, **19**, 1675–1685.
18 J. W. Jung, H. W. Kang, T. Y. Kang, J. H. Park, J. Park and D. W. Cho, *Int. J. Precis. Eng. Man.*, 2012, **13**, 445–449.
19 V. Mironov, T. Boland, T. Trusk, G. Forgacs and R. R. Markwald, *Trends Biotechnol.*, 2003, **21**, 157–161.
20 J. H. Shim, J. Y. Kim, J. K. Park, S. K. Hahn, J. W. Rhie, S. W. Kang, S. H. Lee and D. W. Cho, *J. Biomater. Sci., Polym. Ed.*, 2010, **21**, 1069–1080.
21 R. d'Aquino, A. Graziano, M. Sampaolesi, G. Laino, G. Pirozzi, A. De Rosa and G. Papaccio, *Cell Death Differ.*, 2007, **14**, 1162–1171.
22 A. Graziano, R. d'Aquino, G. Laino and G. Papaccio, *Stem Cell Rev.*, 2008, **4**, 21–26.
23 S. Gronthos, M. Mankani, J. Brahim, P. G. Robey and S. Shi, *Proc. Natl. Acad. Sci. U. S. A.*, 2000, **97**, 13625–13630.
24 Y. Y. Jo, H. J. Lee, S. Y. Kook, H. W. Choung, J. Y. Park, J. H. Chung, Y. H. Choung, E. S. Kim, H. C. Yang and P. H. Choung, *Tissue Eng.*, 2007, **13**, 767–773.
25 L. Wang, M. Yan, Y. Wang, G. Lei, Y. Yu, C. Zhao, Z. Tang, G. Zhang, C. Tang, J. Yu and H. Liao, *Cell Proliferation*, 2013, **46**, 214–222.
26 K. Hara, Y. Yamada, S. Nakamura, E. Umemura, K. Ito and M. Ueda, *J. Endodont.*, 2011, **37**, 1647–1652.
27 J. H. Shim, J. S. Lee, J. Y. Kim and D. W. Cho, *J. Micromech. Microeng.*, 2012, 22.
28 S. H. Lee, Y. S. Sohn, Y. W. Choi, N. H. Park and H. J. Yoon, *Tissue Eng. Regener. Med.*, 2010, **7**, 248–254.
29 Á. E. Mercado-Pagán, A. M. Stahl, Y. Shanjani and Y. Z. Yang, *Ann. Biomed. Eng.*, 2015, **43**, 718–729.
30 O. Tsigkou, I. Pomerantseva, J. A. Spencer, P. A. Redondo, A. R. Hart, E. O'Doherty, Y. Lin, C. C. Friedrich, L. Daheron, C. P. Lin, C. A. Sundback, J. P. Vacanti and C. Neville, *Proc. Natl. Acad. Sci. U. S. A.*, 2010, **107**, 3311–3316.
31 C. M. Ogilvie, C. Lu, R. Marcucio, M. Lee, Z. Thompson, D. Hu, J. A. Helms and T. Miclau, *Iowa Orthop. J.*, 2012, **32**, 90–94.
32 J. M. Kanczler and R. O. Oreffo, *Eur. Cells Mater.*, 2008, **15**, 100–114.
33 D. H. Kempen, L. Lu, A. Heijink, T. E. Hefferan, L. B. Creemers, A. Maran, M. J. Yaszemski and W. J. Dhert, *Biomaterials*, 2009, **30**, 2816–2825.
34 Y. Amo, M. Masuzawa, Y. Hamada and K. Katsuoka, *Br. J. Dermatol.*, 2004, **150**, 160–161.
35 L. E. Benjamin and E. Keshet, *Proc. Natl. Acad. Sci. U. S. A.*, 1997, **94**, 8761–8766.
36 N. Srabovic, Z. Mujagic, J. Mujanovic-Mustedanagic, A. Softic, Z. Muminovic, A. Rifatbegovic and L. Begic, *Int. J. Breast Cancer*, 2013, **2013**, 746749.